2018

One dimensional hierarchical nanostructures composed of CdS nanosheets/nanoparticles and Ag nanowires with promoted photocatalytic performance

Jinyan Xiong
Wuhan Textile University, Soochow University, University of Wollongong, jx513@uowmail.edu.au

Xulei Du
East China University of Science and Technology

Gang Cheng
Chonbuk National University, Wuhan Institute of Technology

Huagui Yang
East China University of Science and Technology

Jun Chen
University of Wollongong, junc@uow.edu.au

See next page for additional authors

Publication Details

Xiong, J., Du, X., Cheng, G., Yang, H., Chen, J., Dou, S. & Li, Z. (2018). One dimensional hierarchical nanostructures composed of CdS nanosheets/nanoparticles and Ag nanowires with promoted photocatalytic performance. Inorganic Chemistry Frontiers, 5 (4), 903-915.

One dimensional hierarchical nanostructures composed of CdS nanosheets/nanoparticles and Ag nanowires with promoted photocatalytic performance

Abstract
Constructing one-dimensional (1D) hierarchical photocatalysts is deemed to be central to promoting photocatalytic capacity. In this paper, 1D hierarchical structures composed of CdS nanosheets/nanoparticles on Ag nanowires (denoted as 1D Ag@CdS core-shell hierarchical hetero-nanowires) have been fabricated via a wet-chemistry approach at low temperature. The optimization of the synthetic parameters indicates that the amounts of Cd(NO 3) 2 ·4H 2 O and thiourea play important roles in the construction of the 1D hierarchical structures. The as-prepared 1D hierarchical Ag@CdS core-shell hetero-nanowires exhibit efficient photocatalytic performance in both methyl orange (MO) degradation (degrade 96% of MO within 240 min) and hydrogen generation (73.5 μmol h -1) from water splitting due to the unique hybrid nano-architecture. It is expected that this Ag@CdS hierarchical nanostructure could have potential in solar energy conversion and this fabrication technique could be used as a reference to design other 1D metal@semiconductor core-shell heteronanowires.

Disciplines
Engineering | Physical Sciences and Mathematics

Publication Details
Xiong, J., Du, X., Cheng, G., Yang, H., Chen, J., Dou, S. & Li, Z. (2018). One dimensional hierarchical nanostructures composed of CdS nanosheets/nanoparticles and Ag nanowires with promoted photocatalytic performance. Inorganic Chemistry Frontiers, 5 (4), 903-915.

Authors
Jinyan Xiong, Xulei Du, Gang Cheng, Huagui Yang, Jun Chen, Shi Xue Dou, and Zhen Li

INORGANIC CHEMISTRY
FRONTIERS

RESEARCH ARTICLE

View Article Online
View Journal | View Issue

Cite this: *Inorg. Chem. Front.*, 2018, **5**, 903

One dimensional hierarchical nanostructures composed of CdS nanosheets/nanoparticles and Ag nanowires with promoted photocatalytic performance

Jinyan Xiong,[a,b,c] Xulei Du,[d] Gang Cheng,[e] Huagui Yang,[d] Jun Chen,[f] Shixue Dou[c] and Zhen Li *[b,c]

Received 7th January 2018,
Accepted 8th February 2018

DOI: 10.1039/c8qi00014j

rsc.li/frontiers-inorganic

Constructing one-dimensional (1D) hierarchical photocatalysts is deemed to be central to promoting photocatalytic capacity. In this paper, 1D hierarchical structures composed of CdS nanosheets/nanoparticles on Ag nanowires (denoted as 1D Ag@CdS core–shell hierarchical hetero-nanowires) have been fabricated *via* a wet-chemistry approach at low temperature. The optimization of the synthetic parameters indicates that the amounts of $Cd(NO_3)_2{\cdot}4H_2O$ and thiourea play important roles in the construction of the 1D hierarchical structures. The as-prepared 1D hierarchical Ag@CdS core–shell hetero-nanowires exhibit efficient photocatalytic performance in both methyl orange (MO) degradation (degrade 96% of MO within 240 min) and hydrogen generation (73.5 μmol h^{-1}) from water splitting due to the unique hybrid nano-architecture. It is expected that this Ag@CdS hierarchical nanostructure could have potential in solar energy conversion and this fabrication technique could be used as a reference to design other 1D metal@semiconductor core–shell heteronanowires.

Introduction

During the past decades, considerable interest has been paid to semiconductor-based photocatalysis because of its wide applications in renewable energy and environmental remediation and protection.[1–7] The overall performance of photocatalysts strongly relies on many microscopic structural and morphological factors.[8–12] Recently, the engineering of biomimetic photocatalysts has been gaining immense attention inspired by the photochemical processes in nature.[13,14] It is well known that the unique natural hierarchical heterostructure of branches with green leaves is beneficial for the highly efficient conversion of sunlight into chemical energy through the photosynthetic process. In the natural photosynthetic system, the two-dimensional (2D) leaves with optimized surface area and packing density can enhance the light absorption and surface reactions, and the one-dimensional (1D) branch can transport nutrition to the leaves for their biofunctions and reactions. Therefore, it is speculated that the similar artificial 1D hierarchical nanostructured materials with high specific surface area, short diffusion paths to active surface sites, excellent electron transport property, and high surface-to-volume ratio could achieve improved photoenergy conversion efficiency.[9,10,13,15–22]

CdS is one such attractive visible-light-driven photocatalyst with a small band gap (2.4 eV), which makes it an appealing candidate for application in hydrogen production and organic pollutant degradation.[15,23–27] The inherent limitation of the fast recombination of photogenerated electron–hole pairs, however, leads to a low photocatalytic efficiency.[25,26] To enhance the lifetime of the photogenerated carriers, modification of CdS with novel plasmonic metals (*e.g.*, Ag, Au, Pd, and Pt) has been demonstrated to be an effective strategy.[25,26,28–34] Compared with other noble metals, Ag is more attractive because of its high electrical and thermal conductivity, antibacterial characteristics, low cost, and nontoxicity. Ag nanostructures exhibit a wealth of optical and photoelectrochemical properties directly related to their geometry-

[a]*College of Chemistry and Chemical Engineering, Hubei Key Laboratory of Biomass Fibers and Eco-dyeing & Finishing, Wuhan Textile University, Wuhan 430200, China*
[b]*State Key Laboratory of Radiation Medicine and Protection, School of Radiation Medicine and Radiation Protection, Collaborative Innovation Center of Radiation Medicine of Jiangsu Higher Education Institutions, Soochow University, 199 Ren Ai Road, Suzhou Industrial Park, Suzhou 215123, China. E-mail: zhenli@suda.edu.cn; Fax: +86-512-65882931; Tel: +86-512-65882931*
[c]*Institute for Superconducting & Electronic Materials, The University of Wollongong, NSW 2500, Australia*
[d]*Key Laboratory for Ultrafine Materials of Ministry of Education, School of Materials Science and Engineering, East China University of Science and Technology, 130 Meilong Road, Shanghai 200237, China*
[e]*School of Chemistry and Environmental Engineering, Wuhan Institute of Technology, Xiongchu Avenue, Wuhan, 430073, PR China*
[f]*Intelligent Polymer Research Institute, The University of Wollongong, NSW 2500, Australia*

dependent surface plasmon resonances, which makes 1D Ag nanostructures more attractive in the field of photocatalysis.[35–37] The Ag nanowires (NWs) in the photocatalysts serve as an express way to efficiently transport electrons, leading to a low recombination of photogenerated electron–hole pairs and an improved photocatalytic activity. Therefore, the synthesis of heterostructures integrating Ag NWs with other functional semiconductor photocatalysts has been widely exploited in recent years, such as Ag-AgCl,[38] Ag-Ag_3PO_4,[39] Ag-TiO_2,[40] Ag-Cu_2O,[36] and Ag-ZnO.[41] Although there are a few reports on the degradation of organic pollutants by Ag-CdS hybrids,[25,26] there is still no report on highly efficient heterostructured photocatalysts based on a 1D Ag@CdS core–shell hierarchical architecture, which might be able to fully take advantage of the 1D hierarchical nanostructure.

Inspired by the hierarchical structure of the natural photosynthetic system, 1D Ag@CdS core–shell photocatalysts with hierarchical nanostructures were prepared by a simple wet chemistry approach in this work. The structure and morphology of the as-prepared Ag@CdS core–shell photocatalysts can be tailored by simply controlling the amounts of $Cd(NO_3)_2{\cdot}4H_2O$/thiourea. Moreover, their photocatalytic activity was evaluated by the degradation of methyl orange (MO) and hydrogen production, and the 1D hierarchical Ag@CdS NWs showed better photocatalytic performance compared with pure CdS, which could result from their specific hierarchical nanostructures and proper constitution.

Experimental section

Materials

Silver nitrate ($AgNO_3$), sodium chloride (NaCl), polyvinylpyrrolidone (PVP40), cadmium nitrate tetrahydrate ($Cd(NO_3)_2{\cdot}4H_2O$), thiourea (CH_4N_2S), ammonium hydroxide solution (28%–30% NH_3 basis), Na_2SO_3, Na_2S, and methyl orange (MO) were purchased from Sigma-Aldrich. 1,2-Propanediol and sodium hydroxide were purchased from Alfa Aesar. All of the chemicals were analytical grade and used directly without further purification.

Sample preparation

Ag nanowires (Ag NWs) were fabricated according to our reported method.[41] In a typical synthesis, 10 mL of 1,2-propanediol containing PVP40 was loaded into a 25 mL vial and heated with magnetic stirring in an oil bath at 135 °C for 1 h. NaCl was then quickly added, and the stirring was continued for another 5 min, followed by the addition of $AgNO_3$ solution. The mixed solution was then heated at 135 °C with magnetic stirring for 1 h, yielding the grey Ag NWs.

Core–shell Ag@CdS hierarchical hetero-nanowires were synthesized by a simple solution process. Typically, 1.2 mmol of $Cd(NO_3)_2{\cdot}4H_2O$ and 0.6 mmol of thiourea were added into 8 mL of freshly prepared Ag NW solution under constant magnetic stirring for 30 min, and then 1 mL of $NH_3{\cdot}H_2O$ was added into the above reaction mixture with stirring for another 5 min. Next, the solution was stirred at 80 °C in an oil bath for 1 h and then the resultant samples were separated by centrifugation, washed with Milli-Q water and absolute ethanol to remove impurities, and then dried at 60 °C (A1). Other samples (A2–A17) were also prepared under identical conditions by varying the amounts of $Cd(NO_3)_2{\cdot}4H_2O$/thiourea. The detailed experimental parameters are listed in Table 1.

Pure CdS nanostructures were prepared using a similar procedure to that for Ag@CdS core–shell hetero-nanowires, except that 1,2-propanediol was added rather than the Ag NW solution.

Characterization

The X-ray diffraction (XRD) measurements were performed on a GBC MMA X-ray diffractometer using Cu $K\alpha_1$ radiation (40 kV). The XRD patterns were recorded from 20° to 80° with a scanning rate of 4° min^{-1}. The scanning electron microscopy (SEM) images were collected using a field-emission scanning electron microscope (JSM-7500FA, JEOL) operated at an accelerating voltage of 5 kV. The transmission electron microscopy (TEM) images and EDX spectrum were collected on a field-emission transmission electron microscope (ARM-200F, JEOL), using an accelerating voltage of 200 kV. The ultraviolet/visible (UV/vis) absorption spectra were collected at room temperature on a UV-3600 (Shimadzu) spectrometer. The Brunauer–Emmett–Teller (BET) specific surface areas of the as-synthesized samples were analyzed by nitrogen adsorption in a Micromeritics ASAP 2020 nitrogen adsorption apparatus (USA). Photoluminescence spectra (PL) were recorded with a HITACHI F4600 fluorescence spectrophotometer.

Photocatalytic test

The photodegradation of MO over the as-synthesized Ag@CdS core–shell hybrids was evaluated under irradiation with a LSC-100 Solar Simulator (Newport). In an experiment, 20 mg of photocatalyst was added into 50 mL of MO solution (10 mg L^{-1}) at room temperature. Prior to irradiation, the sus-

Table 1 The experimental conditions for the synthesis of Ag@CdS core–shell hetero-nanowires

Sample	Ag NWs (mL)	$Cd(NO_3)_2{\cdot}4H_2O$ (mmol)	Thiourea (mmol)	$NH_3{\cdot}H_2O$ (mL)
A1	8	1.2	0.6	1
A2	8	1.2	0.6	—
A3	8	0.3	0.6	1
A4	8	0.6	0.6	1
A5	8	1.8	0.6	1
A6	8	2.4	0.6	1
A7	8	1.2	1.2	1
A8	8	1.2	2.4	1
A9	8	0.075	0.075	1
A10	8	0.15	0.15	1
A11	8	0.3	0.3	1
A12	8	0.15	0.075	1
A13	8	0.075	0.15	1
A14	8	0.3	0.15	1
A15	8	0.15	0.3	1
A16	8	0.6	0.3	1
A17	8	0.3	0.6	1

pension was stirred in the dark to ensure the establishment of an adsorption–desorption equilibrium between the photocatalyst and the MO. Then, the solution was exposed to solar light irradiation under magnetic stirring. At each irradiation time interval, 2 mL of the suspension was collected and then centrifuged to remove the photocatalyst. The concentration of MO was analysed by a Shimadzu UV-3600 spectrophotometer, and the characteristic absorption of MO at 464 nm was used to evaluate its photocatalytic degradation. All of the measurements were carried out at room temperature.

The hydrogen evolution reaction over the as-synthesized Ag@CdS core–shell hybrids was performed in a glass gas-closed-circulation system with a top irradiation-type reaction vessel (LabSolar H_2). A 300 W Xenon lamp (Perfect, China) with a 420 nm cut-off filter ($\lambda \geq 420$ nm) was used as a visible-light source. The temperature of the reactant solution was maintained at 20 °C by a flow of cooling water during the test. In a typical experiment, 30 mg of photocatalyst was added into 50 mL of aqueous solution containing 0.25 M Na_2SO_3 and 0.35 M Na_2S as sacrificial reagents. Prior to the hydrogen evolution reaction, the system was evacuated by a pump and stirred for 30 min to remove the dissolved air in the water. The amount of hydrogen gas was automatically analyzed by on-line gas chromatography (GC-2014C) with a thermal conductivity detector (TCD) and 5A molecular sieve capillary column.

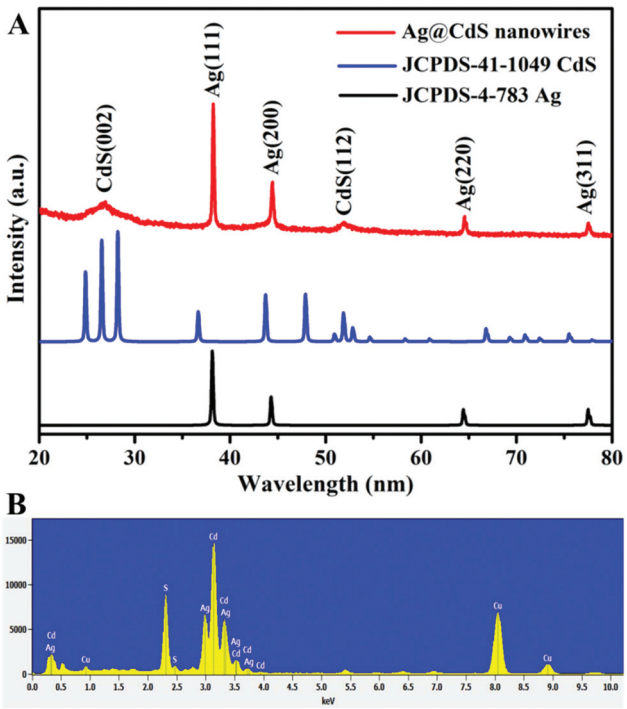

Fig. 1 (A) XRD pattern and (B) EDX spectrum of the as-prepared Ag@CdS heterostructures (A1), for which the added amount of $Cd(NO_3)_2{\cdot}4H_2O$/thiourea was 1.2 mmol/0.6 mmol, respectively.

Results and discussion

The phase compositions and purities of the as-prepared products were characterized by X-ray diffraction (XRD). Fig. 1A shows a typical XRD pattern of the as-prepared A1 sample prepared from $Cd(NO_3)_2{\cdot}4H_2O$ (1.2 mmol) and thiourea (0.6 mmol), all of the diffraction peaks could be indexed to those of hexagonal wurtzite CdS (JCPDS No. 41-1049) and face-centred-cubic Ag (JCPDS card No. 04-0783). The lack of other peaks in the XRD pattern indicates the high purity of the products. The elemental compositions of the as-prepared samples were determined by energy dispersive X-ray (EDX) spectroscopy. As shown in Fig. 1B, the EDX spectrum displays strong peaks of the Ag, Cd, and S elements with weight percentages of 24.73%, 56.16%, and 19.11%, respectively. The atomic ratio of Ag : Cd : S was quantified to be 1 : 2.2 : 2.6, indicating a Ag/CdS composition. The strong Cu peak comes from the copper grid used for the TEM characterization. These results confirmed the successful synthesis of the Ag@CdS hybrid.

Characterizations by scanning electron microscopy (SEM) and transmission electron microscopy (TEM) provide insights into the morphology and detailed structure of the as-prepared Ag@CdS hybrid. A panoramic view of the as-prepared sample shows uniform hierarchical nanowire structures (Fig. 2A). The enlarged SEM image in Fig. 2B clearly reveals dense growth of many interleaved nanosheets and a few nanoparticles over the entire surface of the 1D nanowire to form a hierarchical nanostructure with no visible individual or isolated CdS nanosheets or nanoparticles. Fig. 2C clearly shows the TEM image of an individual Ag@CdS hierarchical nanostructure, in which sheet-like leaves surround the 1D nanowire to construct a hierarchical core–shell architecture. The hybrid shows strong contrast between the boundary and the centre of the composite, in which the darker core is metallic Ag, and the brighter shell would be semiconducting CdS. The high-resolution TEM (HRTEM) image in Fig. 2D shows lattice fringes with a spacing of 0.33 nm, which corresponds to the (002) planes of the hexagonal wurtzite CdS. High-angle annular dark-field (HAADF) imaging was used to identify each chemical component. Due to the differences among Ag, S and Cd in scattering electrons, the as-prepared Ag@CdS hybrid has different contrasts in the HAADF image (Fig. 2E), which are opposite to those observed in the bright field image, *i.e.* the bright segments indicate the presence of the heavier metal Ag and the dark parts indicate the presence of CdS.

Furthermore, the distribution of elements in the Ag@CdS core–shell hetero-nanowires was studied with energy-dispersive X-ray (EDX) elemental mapping [Fig. 2(F–H)]. The HAADF-TEM image in Fig. 2(E) is the area where the elemental mapping was obtained. The blue, pink, and yellow colors represent the distributions of silver, sulfur, and cadmium, respectively. The presence of the three elements in the nanowires is in agreement with the proposed Ag@CdS composition. The spatial distribution of the colors verifies the core–shell structure, where the element Ag is located in the core and the elements S and Cd of CdS are distributed on the outside of the shell.

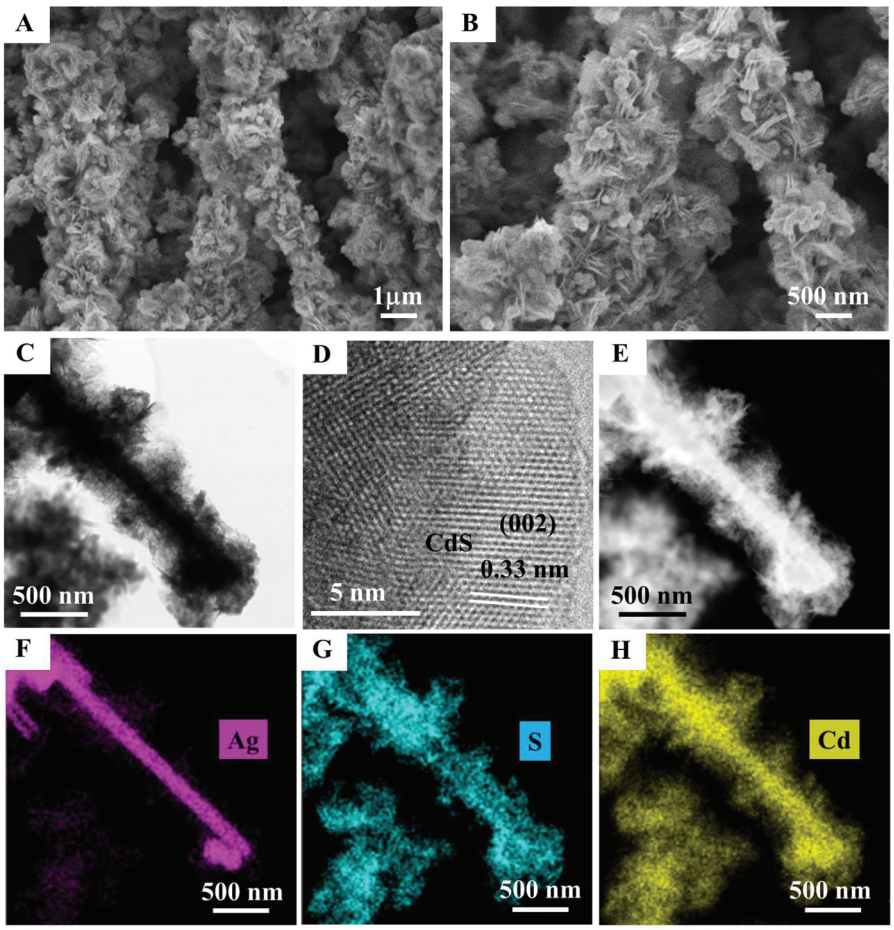

Fig. 2 (A and B) The SEM images of the as-prepared Ag@CdS heterostructures (A1) when the added amount of $Cd(NO_3)_2{\cdot}4H_2O$/thiourea is 1.2 mmol/0.6 mmol; (C) the TEM image, (D) the HRTEM image, (E) the HAADF, and (F–H) the corresponding EDX elemental mapping analysis of an individual Ag@CdS heterostructure.

The optical properties of the Ag@CdS heterostructures have been studied by analyzing the UV-vis absorption spectra (see Fig. 3). Remarkably, the surface plasmon resonance (SPR) absorption bands of the Ag NWs are significantly weakened and broadened, and there is a new characteristic absorption feature of the CdS crystals with a weak band-gap absorption band at around 490 nm, which is similar to the reported 489 nm adsorption of CdS NWs[42] and 468–496 nm adsorption of CdS nanoparticles.[43] The spectral results observed herein could possibly reflect contributions to the synergistic effects between the Ag NWs and CdS shell in the Ag@CdS hybrids and provide strong evidence that the Ag NWs have essentially turned into Ag@CdS hybrids, with the product mainly composed of the CdS component,[44] as well as suggesting that the good contact between the Ag core and CdS shell might ensure effective charge transfer across the phase boundary and cause changes in the structure and shape of the product.[45,46] Their broad absorbance from the UV to the near-infrared window is crucial for the full use of sunlight.

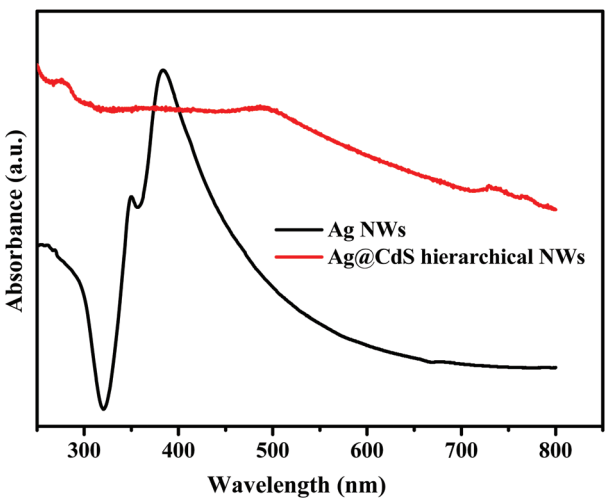

Fig. 3 The UV-Vis absorption spectra of Ag NWs and the as-prepared Ag@CdS heterostructures (A1) with added amounts of $Cd(NO_3)_2{\cdot}4H_2O$/thiourea of 1.2 mmol/0.6 mmol.

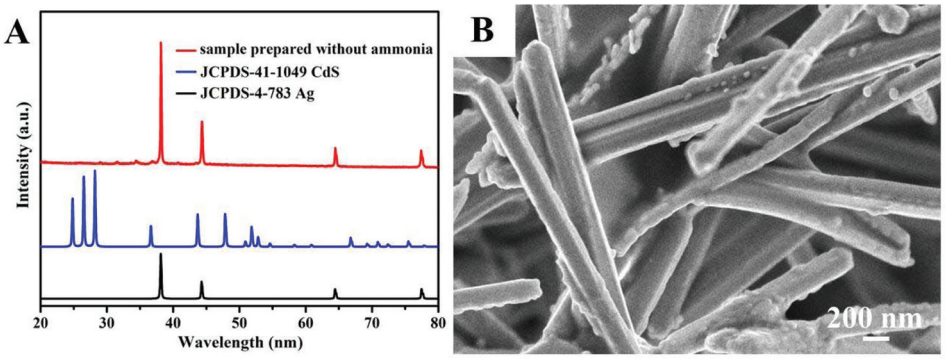

Fig. 4 (A) The XRD pattern and (B) the SEM image of the product (A2) prepared without ammonia with added amounts of $Cd(NO_3)_2{\cdot}4H_2O$/thiourea of 1.2 mmol/0.6 mmol.

Interestingly, it was found that the addition of ammonia, $Cd(NO_3)_2{\cdot}4H_2O$, and thiourea play important roles in the construction of such 1D hierarchical nanostructures assembled from nanosheets and nanoparticles on nanowires. As shown in Fig. 4, these structures couldn't be formed without addition of ammonia into the reaction system. This is due to the fact that thiourea does not easily decompose to release S at low temperature. But under the basic conditions introduced by ammonia, it can decompose at the reaction temperature.

The controlled experiments have also shown that the amounts of $Cd(NO_3)_2{\cdot}4H_2O$ and thiourea are crucial to the formation of well-defined 1D hierarchical nanostructures assembled from nanosheets and nanoparticles. For instance, when the amount of $Cd(NO_3)_2{\cdot}4H_2O$ was decreased from 1.2 mmol to 0.3 mmol (Fig. 5A) and 0.6 mmol (Fig. 5B) while keeping the other experimental conditions unchanged, the morphology of the products significantly changed. As shown in Fig. 5A and B, the Ag NWs are coated with many densely packed CdS nanoparticles. When the amount of $Cd(NO_3)_2{\cdot}4H_2O$ was further increased to 1.8 mmol (Fig. 5C) and 2.4 mmol (Fig. 5D), 1D hierarchical nanowires assembled from nanosheets and nanoparticles were obtained, which are similar to the product prepared in the presence of 1.2 mmol $Cd(NO_3)_2{\cdot}4H_2O$ (Fig. 2A and B). Moreover, it was also found that the morphology of the 1D hierarchical nanowires was also sensitive to the amounts of thiourea. When the amount of thiourea was increased from 0.6 mmol to 1.2 mmol and 2.4 mmol, there were many nanoparticles and flower-like nanospheres constructed by intervolved nanosheets (Fig. 5E and F).

In addition, as shown in Fig. 6A–C, only 1D NWs with many nanoparticles on the surfaces were obtained when keeping the ratio of $Cd(NO_3)_2{\cdot}4H_2O$/thiourea at 1 : 1, and the amounts of $Cd(NO_3)_2{\cdot}4H_2O$ were 0.075, 0.15, and 0.3 mmol, respectively. The TEM images in Fig. 6D–F provide further evidence for the nature of the above representative product, in which the 1D core–shell nanowires can be clearly observed with nanoparticles covering the surface of the Ag NWs. It can also be seen that the shell thickness increased with increasing amounts of reagents in the system. Nevertheless, the morphologies could not be significantly changed by increasing the amount of $Cd(NO_3)_2{\cdot}4H_2O$ and thiourea. For example, a similar 1D nanowire with nanoparticles on the surface of the Ag NWs was obtained when the amount of $Cd(NO_3)_2{\cdot}4H_2O$ or thiourea was increased to 0.15 mmol, respectively (Fig. 6G and H), while keeping the other experimental conditions the same as for the sample prepared in Fig. 6A. The same phenomena could be observed when the amount of $Cd(NO_3)_2{\cdot}4H_2O$ or thiourea was increased to 0.3 mmol (Fig. 6I and J, compared with Fig. 6B) and 0.6 mmol (Fig. 6K and L, compared with Fig. 6C), respectively. The above results directly indicate that the $Cd(NO_3)_2{\cdot}4H_2O$ and thiourea not only act as Cd and S sources but also as the morphology directors in the reaction process, and larger amounts of $Cd(NO_3)_2{\cdot}4H_2O$ with higher ratios of $Cd(NO_3)_2{\cdot}4H_2O$/thiourea facilitate the formation of well-defined 1D hierarchical nanowires.

To determine the potential applications of the as-synthesized 1D Ag@CdS hierarchical nanowires in photocatalysis, the photodegradation of the organic contaminants and hydrogen generation *via* water splitting over the 1D Ag@CdS hierarchical nanowires were evaluated. For comparison, the Ag NWs, Ag@CdS nanowires with various proportions and morphologies (A4, A9–A11), and pure CdS nanoflowers were also tested under identical experimental conditions. As shown in Fig. 7A, it can be clearly seen that no obvious MO dye photodegradation was detected without any catalysts under solar light irradiation. All the as-prepared Ag@CdS nanostructures exhibit high photocatalytic performance, however, sample A1 showed the highest photocatalytic performance, almost degrading 96% of the MO dye within 240 min, while 85% of the MO dye can be degraded over the pure CdS nanoflowers. In contrast, the Ag@CdS nanowire photocatalysts with various proportions of reagents (A9–A11) show relatively low photocatalytic properties towards MO degradation, which may result from the high ratios of metallic Ag nanowires. The above results clearly indicate that the core–shell constitutions have an important impact on the photocatalytic activity of Ag@CdS. Furthermore, the Ag@CdS nanowires with the same nominal

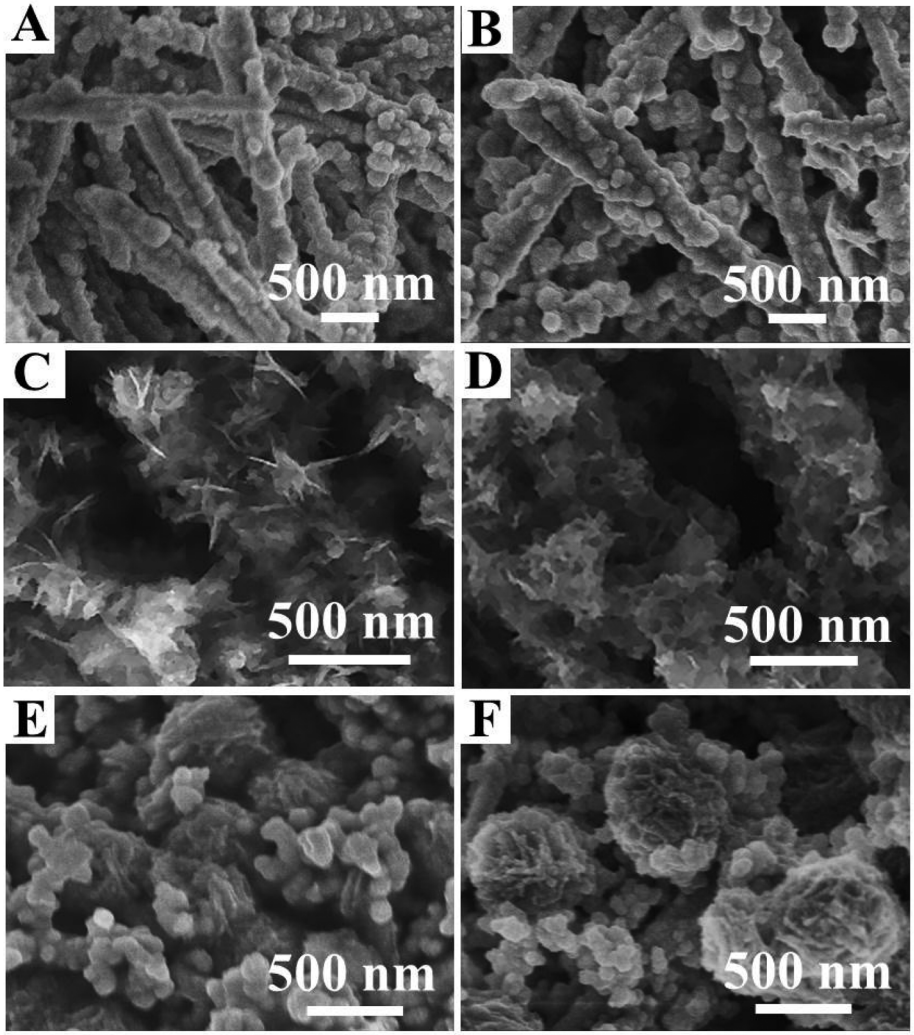

Fig. 5 The SEM images of the product prepared in the presence of different amounts of $Cd(NO_3)_2{\cdot}4H_2O$/thiourea: (A) 0.3 mmol/0.6 mmol, (B) 0.6 mol/0.6 mmol, (C) 1.8 mmol/0.6 mmol, (D) 2.4 mmol/0.6 mmol, (E) 1.2 mmol/1.2 mmol, and (F) 1.2 mmol/2.4 mmol.

1 : 2 ratio (A4) also show relatively low activity for MO degradation, which may be due to the lack of hierarchical structures.

In addition, Fig. 7B shows the hydrogen evolution *via* water splitting of the samples based on aqueous solutions containing 0.25 M Na_2SO_3 and 0.35 M Na_2S sacrificial reagents under visible light irradiation with a 420 nm cut-off filter ($\lambda \geq$ 420 nm). The 1D Ag@CdS hierarchical nanowires (A1) clearly show higher catalytic activity, since the initial rate of hydrogen generation is 73.5 μmol h^{-1} and 181.2 μmol of hydrogen is generated after 4 h, which is about 1.35 times higher than the performance of the pure CdS nanoflowers (17.6 μmol h^{-1}, 134.5 μmol H_2 after 4 h), while the other Ag@CdS with different proportions and morphologies (A4, A9–A11) exhibit relatively low photocatalytic activities, with less than 100 μmol H_2 for the same irradiation time, which is in good agreement with the above photocatalytic activities towards MO degradation. Fig. 7C provides a histogram of the MO degradation rates and hydrogen evolution, which highlights the 1D Ag@CdS hierarchical nanowires (A1) being the best for both reactions.

It is well-known that the specific surface area may contribute to the differences in the photocatalytic performance.[36,47–49] The Brunauer–Emmett–Teller (BET) specific surface area of the synthesized Ag@CdS nanowires with various proportions and morphologies (A1, A4, A9–A11) and pure CdS is investigated by nitrogen adsorption–desorption measurements. Fig. 8 shows the nitrogen adsorption–desorption isotherms of the Ag@CdS nanowires with various proportions and morphologies (A1, A4, A9–A11) and pure CdS. The BET surface area of the hierarchical nanowires (A1) calculated from the results of the N_2 adsorption is 23.71 m^2 g^{-1}, which is larger than that of the particulate CdS-coated heterostructures (10.74, 11.13, 11.29, and 6.05 m^2 g^{-1} for A4, A9, A10 and A11, respectively). The specific hierarchical nanostructure with higher surface area could increase the number of active sites for the photocatalytic

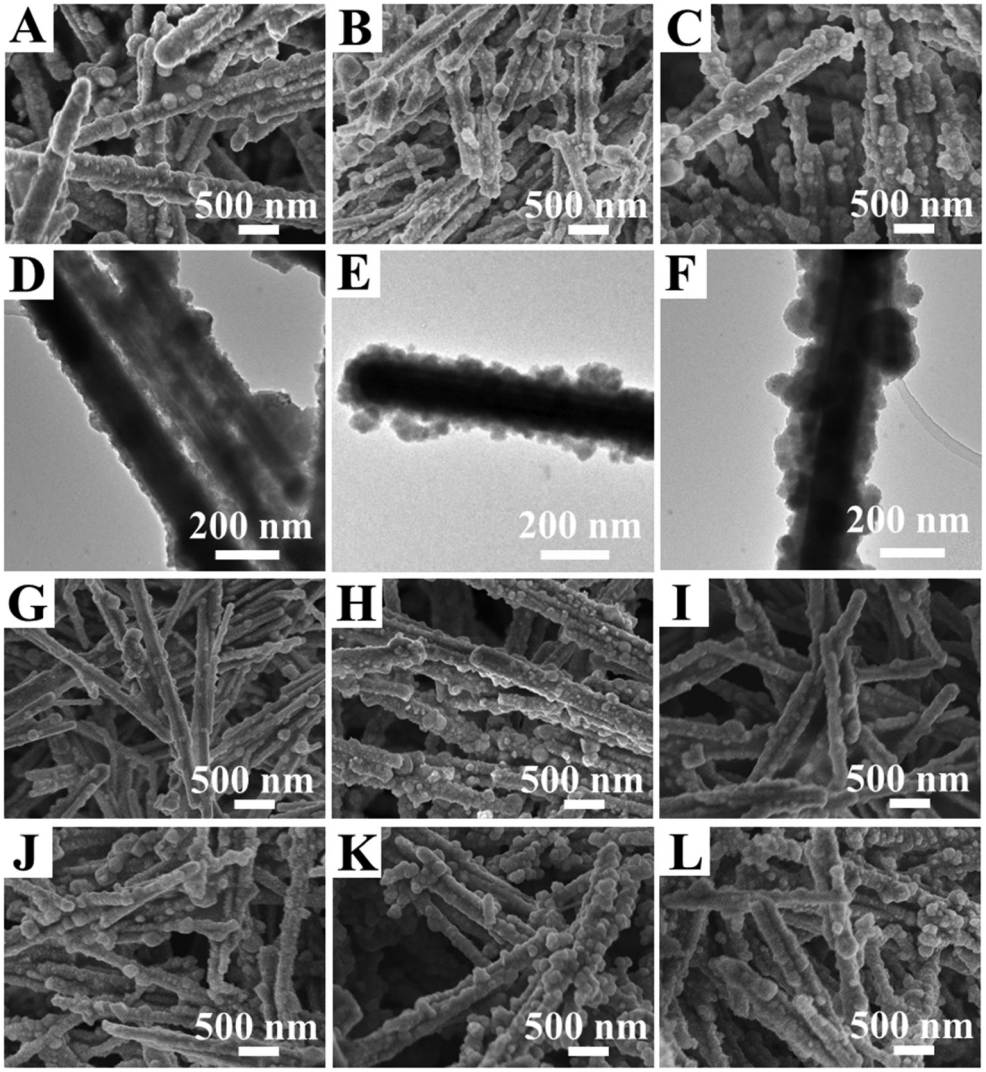

Fig. 6 (A–C, G–L) The SEM images and (D–F) TEM images of the products prepared in the presence of different amounts of $Cd(NO_3)_2{\cdot}4H_2O$/thiourea: (A, D) 0.075 mmol/0.075 mmol, (B, E) 0.15 mmol/0.15 mmol, (C, F) 0.3 mmol/0.3 mmol, (G) 0.15 mmol/0.075 mmol, (H) 0.075 mmol/0.15 mmol, (I) 0.3 mmol/0.15 mmol, (J) 0.15 mmol/0.3 mmol, (K) 0.6 mmol/0.3 mmol, and (L) 0.3 mmol/0.6 mmol.

reaction and thus facilitate diffusion of the reactants and products during the reaction. In addition, the unique hierarchical heterostructures may provide a better anchoring surface in comparison with the relatively smooth surfaces of the particulate coated core–shell heterostructures. Furthermore, the interfacial charge transfer in the hybrid may also account for the enhanced photodegradation performance of MO and hydrogen production. It should be noted that pure CdS has a BET surface area (23.98 $m^2\ g^{-1}$) comparable with Ag@CdS hierarchical nanowires (A1), but shows lower photocatalytic activity, which might be attributed to the rapid recombination of the photoinduced electrons and holes generated by pure CdS.[50–52]

It is well known that the reactive species such as $^{\bullet}O_2^-$, h^+ and $^{\bullet}OH$ played a bridging role in the photodegradation of organic pollutants using semiconductor photocatalysts, and these could vary with different photocatalysts.[53,54] To investigate the photocatalytic mechanism and to understand the better performance of the 1D hierarchical structure composed of CdS nanosheets and Ag nanowires, the effect of the scavengers on the degradation of MO was examined to clarify the contribution of different reductive and oxidative species during the photocatalytic reactions. *P*-Benzoquinone (PBQ), triethanolamine (TEOA), and isopropanol (IPA) were used as scavengers for the $^{\bullet}O_2^-$,[55] h^+,[55] and $^{\bullet}OH$ species,[56] respectively, which were added into the MO solution together with the 1D Ag@CdS hierarchical nanowires before irradiation. As shown in Fig. 9, the complete inhibition of the degradation of MO in the presence of PBQ suggests that $^{\bullet}O_2^-$ is the major reactive species for the photocatalytic degradation of MO. When TEOA was added, the MO photodegradation efficiency significantly decreased from 96% to 55% for the 1D Ag@CdS hierarchical nanowires, which demonstrates that h^+ is the secondary active species in comparison to $^{\bullet}O_2^-$. However, the MO degradation changed slightly after the addition of IPA, indicating that

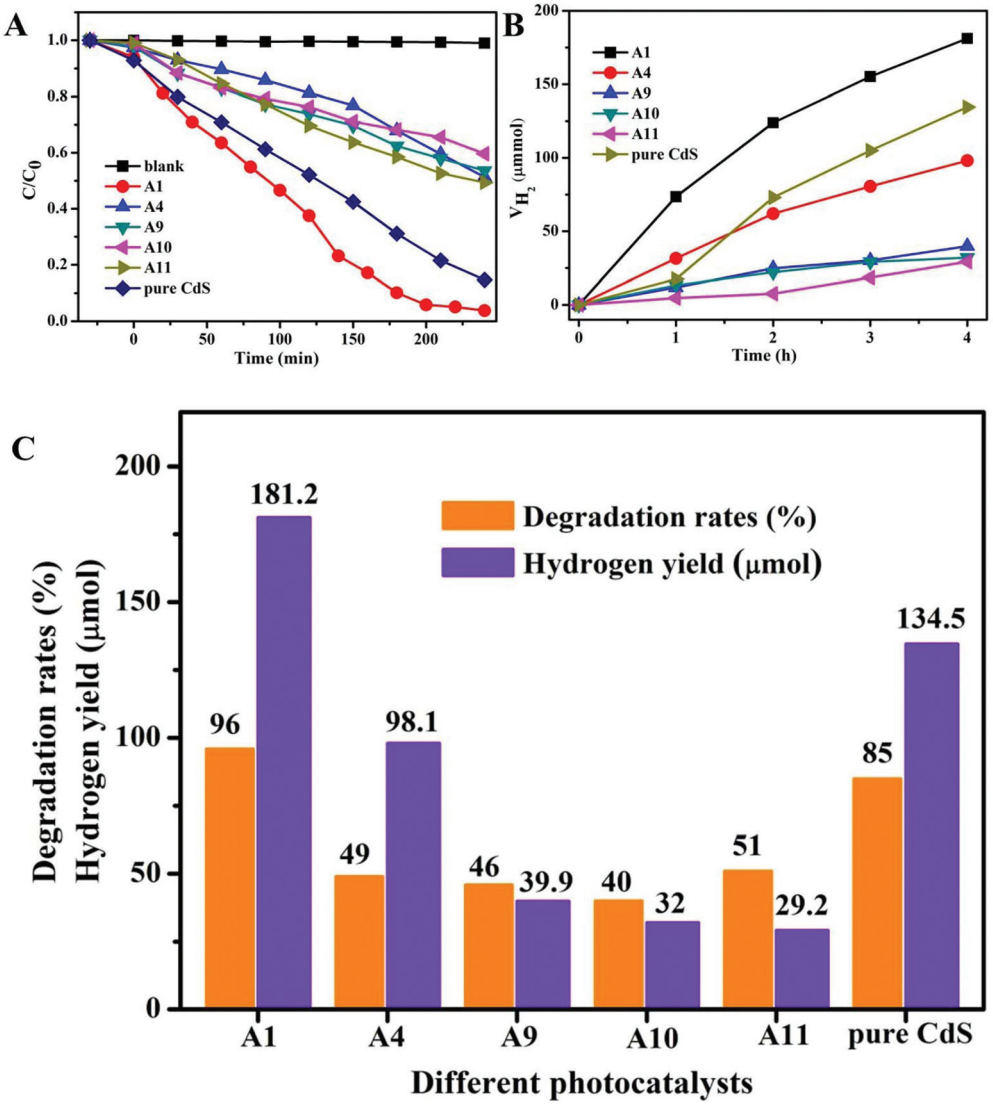

Fig. 7 (A) The photocatalytic activities of the 1D Ag@CdS hierarchical nanowires and other as-prepared photocatalysts towards MO dye degradation under irradiation by solar light. (B) The photocatalytic hydrogen evolution curves of the 1D Ag@CdS hierarchical nanowires and other as-prepared photocatalysts under irradiation by visible light with $\lambda > 420$ nm. (C) The degradation rates and hydrogen yield by various photocatalysts.

$^{\bullet}OH$ had less effect on the photocatalytic reactions. These results illustrate that both $^{\bullet}O_2^-$ and h^+ are the main reactive species for the 1D Ag@CdS hierarchical nanowires in the photocatalytic decolorization of MO under solar light irradiation.

To further clarify the photocatalytic process, the photoluminescence (PL) spectra of the samples were analysed. The PL arises from the recombination of charge carriers, and it is widely used to investigate the migration, transfer, and recombination processes of the photogenerated electron–hole pairs in semiconductors.[57] Fig. 10 represents the room-temperature PL spectra (excitation at 325 nm) of the 1D Ag@CdS hierarchical nanowires and pure CdS, respectively. For the pure CdS nanoflower, an obvious PL emission is observed at around 525 nm, which can be attributed to the excitonic emissions.[26,27] However, the emission is markedly quenched in the 1D Ag@CdS hierarchical nanowires, which is due to the metallic Ag nanowires boosting the separation of the electron–hole pairs and thereby reducing the recombination of charges. This result indicates the successful suppression of the charge recombination, which in turn promotes the photocatalytic degradation. The lower recombination rate of the photogenerated electrons and holes prolongs the lifetime of the photogenerated carriers and thus greatly improves the photocatalytic activity.

The separation efficiency of the electron–hole pairs of the as-synthesized 1D Ag@CdS hierarchical nanowires (A1) and CdS nanoflower was further characterized with photoelectrochemical current (PC) and electrochemical impedance spectroscopy (EIS), where the related electrochemical measurements were performed according to the procedures described in a previous report.[18] As shown in Fig. 11A, a fast photo-

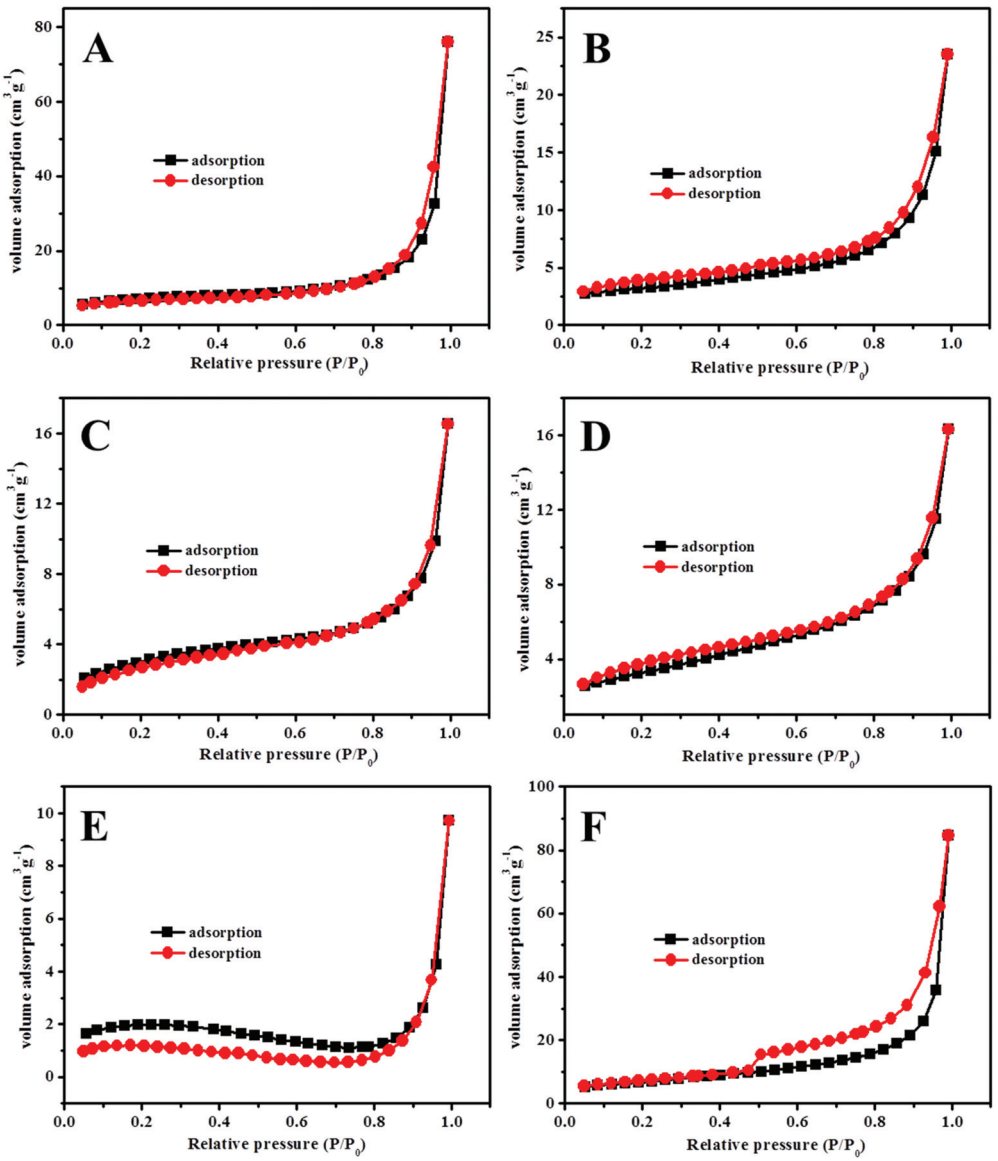

Fig. 8 The nitrogen adsorption–desorption isotherms of the as-synthesized Ag@CdS nanowires with various proportions and morphologies (A1, A4, A9–A11) and pure CdS: (A) A1, (B) A4, (C) A9, (D) A10, (E) A11, and (F) pure CdS.

current response could be observed upon both *light-on* and *light-off* in the two materials. The photocurrent generated by the 1D Ag@CdS hierarchical nanowires is much higher than that of the pure CdS nanoflowers, which reveals the higher separation efficiency of the photoinduced electrons and holes in the 1D Ag@CdS hierarchical nanowires. Fig. 11B shows the EIS Nyquist plots of these two photocatalysts, where the arc radius on the EIS Nyquist plot of the 1D Ag@CdS hierarchical nanowires is smaller than that of the pure CdS nanoflower. The smaller semicircle in the EIS Nyquist plot suggests a fast interfacial charge transfer in the semiconductor.[58,59] This result also demonstrates that the 1D Ag@CdS hierarchical nanowires display superior efficiency compared to that of the CdS nanoflower in separating the electron–hole pairs, which is consistent with the results of PL spectroscopy.

The charge separation effects (forming Schottky junctions by Fermi level equilibration at the metal–semiconductor interfaces) and SPR effects in the 1D Ag@CdS hierarchical nanowires can explain the improved degradation efficiency of MO. The conduction band (CB) energy of CdS is higher than the Fermi energy level of Ag,[26,60] which leads to the fast transfer of the photogenerated electrons from CdS to Ag. Therefore, under the irradiation of a Xe lamp, when more electrons are transferred, fewer photogenerated electrons and holes are recombined, which can greatly improve the efficiency of the charge separation. In this case, MO was degraded directly by the photogenerated holes remaining in the valence band (VB) of CdS or indirectly through the active $^{\bullet}O_2^-$ formed by the photogenerated electrons. The fast transfer of electrons is the main reason for the improved activity.

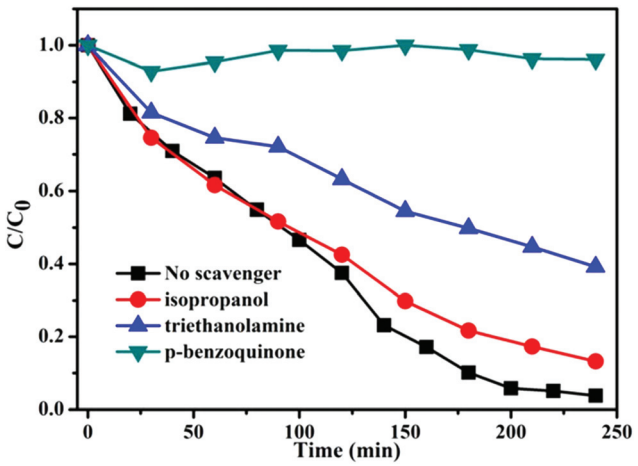

Fig. 9 The photocatalytic degradation of MO over the 1D Ag@CdS hierarchical nanowires in the presence of scavengers.

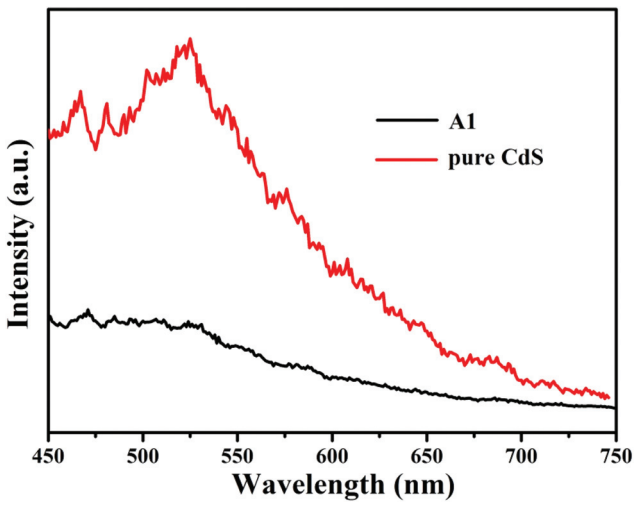

Fig. 10 The room-temperature PL spectra of the 1D Ag@CdS hierarchical nanowires and pure CdS (excitation at 325 nm).

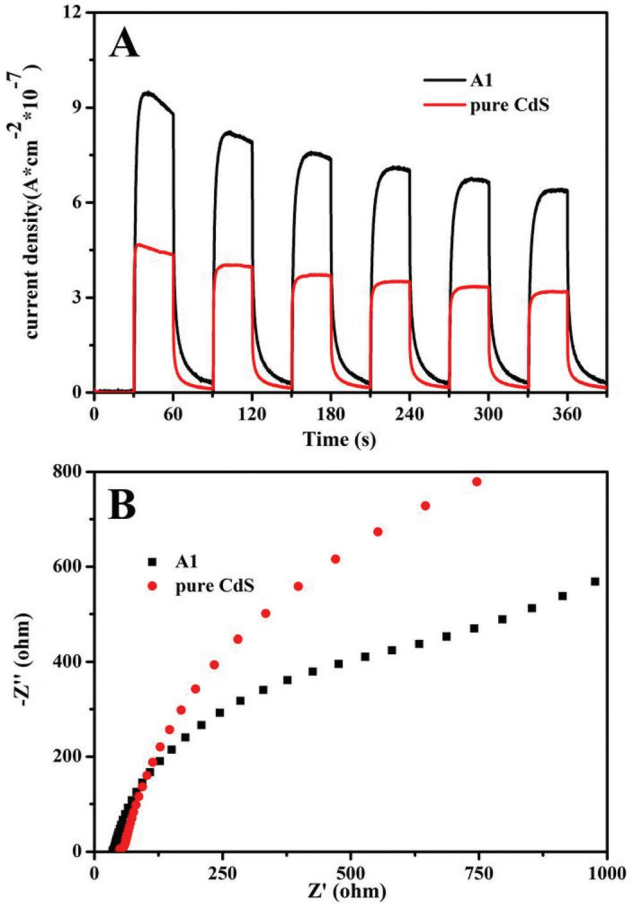

Fig. 11 (A) The photocurrents of the 1D Ag@CdS hierarchical nanowires (A1) and CdS nanoflower under light irradiation at a constant potential; (B) the EIS spectra of the 1D Ag@CdS hierarchical nanowires (A1) and CdS nanoflower.

In addition, the Ag core could absorb resonance photons and generate hot electrons. The excited electrons in the SPR state have sufficient energy and can be directly injected into the CB of CdS. Meanwhile, the holes in the VB of CdS can also transfer to the Ag core to reach energy equilibrium, which prevents the direct recombination of the electrons and holes to increase the photocatalytic efficiency.

On the basis of the above results, the superior photocatalytic performance could be ascribed to the synergetic effects of the large surface area and well-defined morphology, Schottky junction, and SPR effects. Specifically, the core–shell structures have important impact on the photocatalytic activity of Ag@CdS and the construction of unique 1D Ag@CdS hierarchical nanowires with optimized constitution and relatively large specific surface area, and in addition the fast transfer of the photogenerated electrons has been proven to be a successful approach to enhance the photocatalytic performance of CdS.

Conclusion

In summary, 1D Ag@CdS core–shell heteronanowires with hierarchical nanostructures have been fabricated by a facile oil bath approach at low temperature. It was found that the involvement of ammonium hydroxide solution and the mole ratio of cadmium nitrate to thiourea have a significant impact on the formation of such 1D hierarchical nanostructures. The photocatalytic activity of the Ag@CdS nanostructure was evaluated by MO degradation and photocatalytic hydrogen evolution. The result showed that the construction of unique 1D Ag@CdS hierarchical nanowires with optimized constitution and relatively large specific surface area has been proven to be a successful and feasible protocol to enhance the photocatalytic performances of CdS. Such 1D core–shell hierarchical nanostructures could be promising photocatalytic candidates.

Conflicts of interest

There are no conflicts to declare.

Acknowledgements

The authors gratefully acknowledge the financial support from the Australian Research Council (ARC) through the Discovery Projects DP 130102274 and DP130102699 and from ISEM at UOW. Z. Li acknowledges support from the 1000 Plan for Young Talents, Jiangsu Specially Appointed Professorship and the Program of Jiangsu Innovative and Entrepreneurial Talents. The authors also acknowledge the use of the facilities in the UOW Electron Microscopy Centre, with particular thanks to David R. G. Mitchell. The authors are also grateful for support from the Jiangsu Provincial Key Laboratory of Radiation Medicine and Protection and the Priority Academic Development Program of Jiangsu Higher Education Institutions (PAPD). They also thank Dr Tania Silver for critical reading of the manuscript.

References

1 M. R. Hoffmann, S. T. Martin, W. Choi and D. W. Bahnemann, Environmental applications of semiconductor photocatalysis, *Chem. Rev.*, 1995, **95**, 69–96.
2 X. Hu, G. Li and J. C. Yu, Design, fabrication, and modification of nanostructured semiconductor materials for environmental and energy applications, *Langmuir*, 2009, **26**, 3031–3039.
3 X. Wang, K. Maeda, A. Thomas, K. Takanabe, G. Xin, J. M. Carlsson, K. Domen and M. Antonietti, A metal-free polymeric photocatalyst for hydrogen production from water under visible light, *Nat. Mater.*, 2009, **8**, 76–80.
4 Z. Zou, J. Ye, K. Sayama and H. Arakawa, Direct splitting of water under visible light irradiation with an oxide semiconductor photocatalyst, *Nature*, 2001, **414**, 625–627.
5 X. Chen, S. Shen, L. Guo and S. S. Mao, Semiconductor-based photocatalytic hydrogen generation, *Chem. Rev.*, 2010, **110**, 6503–6570.
6 X. Li, J. Yu and M. Jaroniec, Hierarchical photocatalysts, *Chem. Soc. Rev.*, 2016, **45**, 2603–2636.
7 H. Pang, Y. Li, L. Guan, Q. Lu and F. Gao, TiO_2/Ni nanocomposites: Biocompatible and recyclable magnetic photocatalysts, *Catal. Commun.*, 2011, **12**, 611–615.
8 J. Xiong, Z. Jiao, G. Lu, W. Ren, J. Ye and Y. Bi, Facile and Rapid Oxidation Fabrication of BiOCl Hierarchical Nanostructures with Enhanced Photocatalytic Properties, *Chem. Eur. J.*, 2013, **19**, 9472–9475.
9 C. Han, Z. Chen, N. Zhang, J. C. Colmenares and Y.-J. Xu, Hierarchically CdS Decorated 1D ZnO Nanorods-2D Graphene Hybrids: Low Temperature Synthesis and Enhanced Photocatalytic Performance, *Adv. Funct. Mater.*, 2015, **25**, 221–229.
10 T. Zhu, J. Li and Q. Wu, Construction of TiO_2 Hierarchical Nanostructures from Nanocrystals and Their Photocatalytic Properties, *ACS Appl. Mater. Interfaces*, 2011, **3**, 3448–3453.
11 S. Xiong, B. Xi and Y. Qian, CdS Hierarchical Nanostructures with Tunable Morphologies: Preparation and Photocatalytic Properties, *J. Phys. Chem. C*, 2010, **114**, 14029–14035.
12 X. Li, H. Xue and H. Pang, Facile synthesis and shape evolution of well-defined phosphotungstic acid potassium nanocrystals as a highly efficient visible-light-driven photocatalyst, *Nanoscale*, 2017, **9**, 216–222.
13 H. Hu, Z. Jiao, G. Lu, J. Ye and Y. Bi, Enhanced photocatalytic properties of biomimetic Ag/AgCl heterostructures, *RSC Adv.*, 2014, **4**, 31795–31798.
14 Y. Wang, K. Jiang, H. Zhang, T. Zhou, J. Wang, W. Wei, Z. Yang, X. Sun, W.-B. Cai and G. Zheng, Bio-Inspired Leaf-Mimicking Nanosheet/Nanotube Heterostructure as a Highly Efficient Oxygen Evolution Catalyst, *Adv. Sci.*, 2015, **2**, 1500003.
15 C. Wei, C. Cheng, J. Zhao, S. Zheng, M. Hao and H. Pang, Assembling CdS mesoporous nanosheets into 3D hierarchitectures for effective photocatalytic performance, *Dalton Trans.*, 2014, **43**, 5687–5693.
16 T. Zhu, H. B. Wu, Y. Wang, R. Xu and X. W. Lou, Formation of 1D Hierarchical Structures Composed of Ni_3S_2 Nanosheets on CNTs Backbone for Supercapacitors and Photocatalytic H_2 Production, *Adv. Energy Mater.*, 2012, **2**, 1497–1502.
17 G. Tian, Y. Chen, W. Zhou, K. Pan, C. Tian, X.-R. Huang and H. Fu, 3D hierarchical flower-like TiO_2 nanostructure: morphology control and its photocatalytic property, *CrystEngComm*, 2011, **13**, 2994–3000.
18 J. Xiong, Y. Gan, J. Zhu, W. Li, C. Gao, Y. Wei, G. Cheng, Z. Li and S. Dou, Insights into the structure-induced catalysis dependence of simply engineered one-dimensional zinc oxide nanocrystals towards photocatalytic water purification, *Inorg. Chem. Front.*, 2017, **4**, 2075–2087.
19 Y. Wei, G. Cheng, J. Xiong, F. Xu and R. Chen, Positive Ni $(HCO_3)_2$ as a Novel Cocatalyst for Boosting the Photocatalytic Hydrogen Evolution Capability of Mesoporous TiO_2 Nanocrystals, *ACS Sustainable Chem. Eng.*, 2017, **5**, 5027–5038.
20 X. Q. Chen, Y. Bai, Z. Li, L. Z. Wang and S. X. Dou, Ambient Synthesis of One-/Two-Dimensional CuAgSe Ternary Nanotubes as Counter Electrodes of Quantum-Dot-Sensitized Solar Cells, *ChemPlusChem*, 2016, **81**, 414–420.
21 X. Q. Chen, Z. Li, Y. Bai, Q. Sun, L. Z. Wang and S. X. Dou, Room-Temperature Synthesis of $Cu_{2-x}E$ (E=S, Se) Nanotubes with Hierarchical Architecture as High-Performance Counter Electrodes of Quantum-Dot-Sensitized Solar Cells, *Chem. – Eur. J.*, 2015, **21**, 1055–1063.
22 Y. Lu, B. Li, S. Zheng, Y. Xu, H. Xue and H. Pang, Syntheses and Energy Storage Applications of MxSy (M = Cu, Ag, Au) and Their Composites: Rechargeable Batteries and Supercapacitors, *Adv. Funct. Mater.*, 2017, **27**, 1703949.

23 Q. Li, B. Guo, J. Yu, J. Ran, B. Zhang, H. Yan and J. R. Gong, Highly Efficient Visible-Light-Driven Photocatalytic Hydrogen Production of CdS-Cluster-Decorated Graphene Nanosheets, *J. Am. Chem. Soc.*, 2011, **133**, 10878–10884.

24 N. Bao, L. Shen, T. Takata and K. Domen, Self-templated synthesis of nanoporous CdS nanostructures for highly efficient photocatalytic hydrogen production under visible light, *Chem. Mater.*, 2007, **20**, 110–117.

25 H. Cui, Z. Gao, Z. Cui, S. Zhu, Z. Li, Y. Liang and X. Yang, Hydrothermal Synthesis of CdS Layer on Ag Nanowires and its Enhanced Photocatalytic Activity, *Curr. Nanosci.*, 2015, **11**, 633–639.

26 Y. Liu, M. Chi, H. Dong, H. Jia, B. Xu and Z. Zhang, Ag/CdS heterostructural composites: Fabrication, characterizations and photocatalysis, *Appl. Surf. Sci.*, 2014, **313**, 558–562.

27 Z. Yu, B. Yin, F. Qu and X. Wu, Synthesis of self-assembled CdS nanospheres and their photocatalytic activities by photodegradation of organic dye molecules, *Chem. Eng. J.*, 2014, **258**, 203–209.

28 X. Ma, K. Zhao, H. Tang, Y. Chen, C. Lu, W. Liu, Y. Gao, H. Zhao and Z. Tang, New Insight into the Role of Gold Nanoparticles in Au@CdS Core-Shell Nanostructures for Hydrogen Evolution, *Small*, 2014, **10**, 4664–4670.

29 S. Liu and Y.-J. Xu, Efficient electrostatic self-assembly of one-dimensional CdS-Au nanocomposites with enhanced photoactivity, not the surface plasmon resonance effect, *Nanoscale*, 2013, **5**, 9330–9339.

30 I. Majeed, M. A. Nadeem, M. Al-Oufi and M. A. Nadeem, Waterhouse GIN, Badshah A, Metson JB, Idriss H, On the role of metal particle size and surface coverage for photocatalytic hydrogen production: A case study of the Au/CdS system, *Appl. Catal., B*, 2016, **182**, 266–276.

31 N. Kumar, V. K. Komarala and V. Dutta, *In situ* synthesis of Au-CdS plasmonic photocatalyst by continuous spray pyrolysis and its visible light photocatalysis, *Chem. Eng. J.*, 2014, **236**, 66–74.

32 S. Han, L. Hu, N. Gao, A. A. Al-Ghamdi and X. Fang, Efficient Self-Assembly Synthesis of Uniform CdS Spherical Nanoparticles-Au Nanoparticles Hybrids with Enhanced Photoactivity, *Adv. Funct. Mater.*, 2014, **24**, 3725–3733.

33 X. Song, W. Yao, B. Zhang and Y. Wu, Application of Pt/CdS for the Photocatalytic Flue Gas Desulfurization, *Int. J. Photoenergy*, 2012, **2012**, 1–5.

34 N. Zhang, S. Liu, X. Fu and Y.-J. Xu, Fabrication of coenocytic Pd@ CdS nanocomposite as a visible light photocatalyst for selective transformation under mild conditions, *J. Mater. Chem.*, 2012, **22**, 5042–5052.

35 M. Long and W. Cai, Advanced nanoarchitectures of silver/silver compound composites for photochemical reactions, *Nanoscale*, 2014, **6**, 7730–7742.

36 J. Xiong, Z. Li, J. Chen, S. Zhang, L. Wang and S. Dou, Facile Synthesis of Highly Efficient One-Dimensional Plasmonic Photocatalysts through Ag@Cu_2O Core–Shell Heteronanowires, *ACS Appl. Mater. Interfaces*, 2014, **6**, 15716–15725.

37 P. Ramasamy, D.-M. Seo, S.-H. Kim and J. Kim, Effects of TiO_2 shells on optical and thermal properties of silver nanowires, *J. Mater. Chem.*, 2012, **22**, 11651–11657.

38 Y. Bi and J. Ye, In situ oxidation synthesis of Ag/AgCl core-shell nanowires and their photocatalytic properties, *Chem. Commun.*, 2009, 6551–6553.

39 Y. Bi, H. Hu, S. Ouyang, Z. Jiao, G. Lu and J. Ye, Selective growth of Ag_3PO_4 submicro-cubes on Ag nanowires to fabricate necklace-like heterostructures for photocatalytic applications, *J. Mater. Chem.*, 2012, **22**, 14847–14850.

40 B. Cheng, Y. Le and J. Yu, Preparation and enhanced photocatalytic activity of Ag@TiO_2 core-shell nanocomposite nanowires, *J. Hazard. Mater.*, 2010, **177**, 971–977.

41 J. Xiong, Q. Sun, J. Chen, Z. Li and S. Dou, Ambient controlled synthesis of advanced core-shell plasmonic Ag@ZnO photocatalysts, *CrystEngComm*, 2016, **18**, 1713–1722.

42 İ Şişman, Template-Assisted Electrochemical Synthesis of Semiconductor Nanowires, *Nanowires: Implementations Appl.*, 2011, 41–58.

43 S. Mlowe, D. J. Lewis, M. A. Malik, J. Raftery, E. B. Mubofu, P. O'Brien and N. Revaprasadu, Bis (piperidinedithiocarbamato) pyridinecadmium(II) as a single-source precursor for the synthesis of CdS nanoparticles and aerosol-assisted chemical vapour deposition (AACVD) of CdS thin films, *New J. Chem.*, 2014, **38**, 6073–6080.

44 C.-H. Kuo, T.-E. Hua and M. H. Huang, Au Nanocrystal-Directed Growth of Au−Cu_2O Core−Shell Heterostructures with Precise Morphological Control, *J. Am. Chem. Soc.*, 2009, **131**, 17871–17878.

45 H. Duan and Y. Xuan, Synthesis and optical absorption of Ag/CdS core/shell plasmonic nanostructure, *Sol. Energy Mater. Sol. Cells*, 2014, **121**, 8–13.

46 J. Xiong, C. Han, W. Li, Q. Sun, J. Chen, S. Chou, Z. Li and S. Dou, Ambient synthesis of a multifunctional 1D/2D hierarchical Ag-Ag_2S nanowire/nanosheet heterostructure with diverse applications, *CrystEngComm*, 2016, **18**, 930–937.

47 J. Xiong, G. Cheng, G. Li, F. Qin and R. Chen, Well-crystallized square-like 2D BiOCl nanoplates: mannitol-assisted hydrothermal synthesis and improved visible-light-driven photocatalytic performance, *RSC Adv.*, 2011, **1**, 1542–1553.

48 J. Xiong, G. Cheng, F. Qin, R. Wang, H. Sun and R. Chen, Tunable BiOCl hierarchical nanostructures for high-efficient photocatalysis under visible light irradiation, *Chem. Eng. J.*, 2013, **220**, 228–236.

49 L. Chen, T. Ji, L. Brisbin and J. Zhu, Hierarchical Porous and High Surface Area Tubular Carbon as Dye Adsorbent and Capacitor Electrode, *ACS Appl. Mater. Interfaces*, 2015, **7**, 12230–12237.

50 X. Zou, P.-P. Wang, C. Li, J. Zhao, D. Wang, T. Asefa and G.-D. Li, One-pot cation exchange synthesis of 1D porous CdS/ZnO heterostructuresfor visible-light-driven H_2 evolution, *J. Mater. Chem. A*, 2014, **2**, 4682–4689.

51 X. Li, X. Chen, H. Niu, X. Han, T. Zhang, J. Liu, H. Lin and F. Qu, The synthesis of CdS/TiO_2 hetero-nanofibers with

enhanced visible photocatalytic activity, *J. Colloid Interface Sci.*, 2015, **452**, 89–97.

52 L. Zou, H. Wang and X. Wang, High Efficient Photodegradation and Photocatalytic Hydrogen Production of CdS/$BiVO_4$ Heterostructure through Z-Scheme Process, *ACS Sustainable Chem. Eng.*, 2017, **5**, 303–309.

53 M. Yin, Z. Li, J. Kou and Z. Zou, Mechanism Investigation of Visible Light-Induced Degradation in a Heterogeneous TiO_2/Eosin Y/Rhodamine B System, *Environ. Sci. Technol.*, 2009, **43**, 8361–8366.

54 Q. Yuan, L. Chen, M. Xiong, J. He, S.-L. Luo, C.-T. Au and S.-F. Yin, Cu_2O/$BiVO_4$ heterostructures: synthesis and application in simultaneous photocatalytic oxidation of organic dyes and reduction of Cr(VI) under visible light, *Chem. Eng. J.*, 2014, **255**, 394–402.

55 X. Ding, K. Zhao and L. Zhang, Enhanced Photocatalytic Removal of Sodium Pentachlorophenate with Self-Doped Bi_2WO_6 under Visible Light by Generating More Superoxide Ions, *Environ. Sci. Technol.*, 2014, **48**, 5823–5831.

56 J. Zhou, G. Tian, Y. Chen, Y. Shi, C. Tian, K. Pan and H. Fu, Growth rate controlled synthesis of hierarchical Bi2S3/In2S3 core/shell microspheres with enhanced photocatalytic activity, *Sci. Rep.*, 2014, **4**, 4027.

57 L. Wu, S. Fang, L. Ge, C. Han, P. Qiu and Y. Xin, Facile synthesis of Ag@CeO_2 core-shell plasmonic photocatalysts with enhanced visible-light photocatalytic performance, *J. Hazard. Mater.*, 2015, **300**, 93–103.

58 A. Migani and L. Blancafort, Excitonic Interfacial Proton-Coupled Electron Transfer Mechanism in the Photocatalytic Oxidation of Methanol to Formaldehyde on TiO_2(110), *J. Am. Chem. Soc.*, 2016, **138**, 16165–16173.

59 M. Nolan, A. Iwaszuk, A. K. Lucid, J. J. Carey and M. Fronzi, Design of Novel Visible Light Active Photocatalyst Materials: Surface Modified TiO_2, *Adv. Mater.*, 2016, **28**, 5425–5446.

60 S. Huang, Y. Lin, J. Yang, X. Li, J. Zhang, J. Yu, H. Shi, W. Wang and Y. Yu, Enhanced photocatalytic activity and stability of semiconductor by Ag doping and simultaneous deposition: the case of CdS, *RSC Adv.*, 2013, **3**, 20782–20792.